ARHGEF18 participates in Endothelial Cell Mechano-sensitivity in Response to Flow

Surya Prakash Rao Batta, Marc Rio, Corentin Lebot, Céline Baron-Menguy, Robin Le Ruz, Gervaise Loirand, Anne-Clémence Vion

ARHGEF18 participates in Endothelial Cell Mechano-sensitivity in Response to Flow

Surya Prakash Rao Batta[1], Marc Rio[1], Corentin Lebot[1], Céline Baron-Menguy[1], Robin Le Ruz[1], Gervaise Loirand[1], Anne-Clémence Vion[1]

[1]Université de Nantes, CHU Nantes, CNRS, INSERM, l'institut du thorax, F-44000 Nantes, France.

*** Correspondance:**
Anne-Clémence Vion
anne-clemence.vion@univ-nantes.fr

Keywords: endothelial cell, shear stress, guanine exchange factor, mechano-transduction

Abstract

Hemodynamic forces play an important role in vascular network development and homeostasis. In physiological condition, shear stress generated by laminar flow promotes endothelial cells (EC) health and induces their alignment in the direction of flow. In contrast, altered hemodynamic forces induce endothelial dysfunction and lead to the development of vascular disorders such as atherosclerosis and aneurysms. Following mechano-sensor activation, Rho protein-mediated cytoskeletal rearrangement is one of the first steps in transforming flow-induced forces into intracellular signals in EC via guanine nucleotide exchange factors (RhoGEFs) that mediate the spatio-temporal activation of these Rho proteins. Here we identified ARHGEF18 as a flow-sensitive RhoGEF specifically activating RhoA. Both ARHGEF18 expression and activity were controlled by shear stress level. ARHGEF18 promotes EC adhesion, focal adhesion formation and migration. ARHGEF18 localized to the tight junction by interacting with ZO-1 and participated to shear stress-induced EC elongation and alignment via its nucleotide exchange activity and the activation of p38 MAPK. Our study therefore characterized ARHGEF18 as the first flow-sensitive RhoA GEF in ECs, whose activity is essential for the maintenance of intercellular junctions and a properly organized endothelial monolayer under physiological flow conditions.

Introduction

Mechano-sensitivity and mechano-transduction play crucial roles in shaping life. Cells, individually or collectively, need to respond appropriately to mechanical cues coming from their environment to adapt and survive, and to ensure healthy tissue development and homeostasis[4]. In the vascular system, endothelial cells (ECs) are exposed constantly to mechanical strains exerted by blood flow[5,6]. ECs are thus able to sense small variations in the direction, magnitude, and regularity of blood flow-induced shear stress[7,8] and consequently modulate their functions to generate adapted response. This leads, for instance, to arteriogenesis[9], vasculature patterning[10,11] and acute regulation of vessel tone,[12] which are critical for both the development and maintenance of a healthy cardiovascular system. On the opposite, failure of ECs to adapt to changes in blood flow or chronic exposure to abnormal flow is the cause of vascular diseases such as hypertension, atherosclerosis[6,13,14] or intracranial aneurysm formation[15].

In physiological condition, shear stress generated by laminar flow as observed in linear parts of the vascular tree, promotes ECs health and induces their alignment in the direction of flow[16,17]. To do so, ECs use several mechano-sensing mechanisms. Well-studied examples are ion channels[18], primary cilia expressed at the apical surface of cells[19,20], but also include mechano-sensing complexes at cell-cell interface such as the PECAM-1/VEGFRs/VE-cadherin complexe[13] and at cell membrane-extracellular matrix attachment such as focal adhesions and integrins[21]. These sensors and complexes play an essential role in transforming flow-induced physiological forces into intracellular signals ultimately leading to various cellular response ranging from chemokine release, Nitric Oxide production to cell proliferation and junction reorganization Rho protein-mediated actin cytoskeleton reorganization is one of the first steps of this process[22–26], as supported by the overexpression of dominant-negative mutants of RhoA or Rac1 in ECs that prevent their correct elongation and alignment[27]. An increase in Rho protein activity is rapidly induced in ECs upon shear stress exposure, with two peaks of activity at 5 min and 2 hours for RhoA [27,28], and a maximal Rac1 and cdc42 activation at 15 min[16,21]. At longer time point, Rho-GTPases activity is not completely lost but preserves a basal level suggesting their involvement not only in establishing the alignment but also in maintaining it. Shear stress not only controls Rho-GTPases activity but also their localization. Upon physiological shear stress exposure, these Rho-GTPases translocate within minutes, from the cytosol to the plasma membrane where they can meet their partners and act on the cytoskeleton[29]. Activation of Rho proteins consists in their transition from an inactive state (GDP-bound) to an active state (GTP-bound)[30]. By promoting the release of GDP followed by GTP loading, the guanine nucleotide exchange factors of Rho proteins, the RhoGEFs, induced Rho protein activation[31]. The peculiar interest of RhoGEFs is their tissue-specific expression and their signal/temporal-specific activation[32] which place them at the control center of the broad effects of Rho-GTPases in cell biology. Some of those RhoGEFs have been described to be exclusively expressed in ECs, such as FGD5[33],to participate in ECs mechano-sensitivity. The RhoGEFs Tiam1 and Vav2 have been shown to be involved in the rapid activation of Rac1 upon shear stress[34]. The RhoGEF Trio keeps Rac1 active at the downstream side of the EC and is essential for long term flow-induced cell alignment[35] as well as barrier integrity through the formation of a NOTCH1/VE-Cadh/LAR/Trio complex[36]. Lastly, ARHGEF12 has been implicated in force sensing through ICAM and participates in leukocytes rolling and transmigration on ECs[37].

Here, using unbiased RNA screening in ECs, we identify that ARHGEF18 expression and activity are flow sensitive. We demonstrate that ARHGEF18 is a RhoA-specific RhoGEF interacting with ZO1 in ECs. We show that ARHGEF18 participates in ECs alignment in response to flow by controlling p38 MAPK activity, tight junction and focal adhesion formation through its guanine nucleotide exchange activity.

Results

Shear stress regulates ARHGEF18 expression and activity

In order to identify RhoGEFs expression modulated by shear stress (SS), we performed a 3'RNA profiling on endothelial cells (EC) exposed to different SS levels (no flow, Static, 0 dyn/cm^2; pathological Low SS, 3,6 dyn/cm^2, (LSS); physiological SS, 16 dyn/cm^2 (PSS) and pathological High SS, 36 dyn/cm^2, (HSS)) (Fig 1A, MA plot of static vs PSS condition). The identification of *KLF2* as a flow-dependent gene the expression of which was significantly increased by HSS validated our experimental conditions (Fig 1A). Among the genes with differential expression, we identified several RhoGEFs but only *ARHGEF18* expression decreases with increased SS (Fig 1A and suppl 1A). We then confirmed this decrease in *ARHGEF18* mRNA expression in EC with increased SS by qPCR, using *KLF2* mRNA expression as an internal control (Fig 1B and Fig suppl 1B). Surprisingly, contrary to the observed down-regulation of

ARHGEF18 mRNA with increased SS, ARHGEF18 protein level increased in pathological SS conditions (LSS and HSS) compared to physiological condition (PSS) (Fig 1C), suggesting an additional post-transcriptional effect of SS on ARHGEF18 protein level. We then examined the sensitivity of ARHGEF18 activity to SS by pull-down assay using nucleotide-free $RhoA^{G17A}$ and $Rac1^{G15A}$ mutants to trap active RhoGEF[38]. Interestingly, under static condition, we were able to trap ARHGEF18 with the $RhoA^{G17A}$ mutant but not with the $Rac1^{G15A}$ mutant indicating a basal nucleotide exchange activity of ARHGEF18 on RhoA but not on Rac1 (Fig 1D and E (lane1, static condition)), confirming ARHGEF18 specificity for RhoA[39].
As we were unable to trap ARHGEF18 with $Rac1^{G15A}$ mutant, we validated the efficiency of this pull-down assay by blotting proteins that have coprecipitated with Rac^{G15A} with an antibody to Vav, known as a Rac GEFs in EC[40]. We were able to detect Vav in the coprecipitated proteins, thus validating this pull-assay and confirming that ARHGEF18 did not interact with Rac1 (Fig suppl 1C). Interestingly, the amount of ARHGEF18 captured by the $RhoA^{G17A}$ mutant was high in ECs exposed to physiological SS (PSS) compared to pathological SS (LSS and HSS) thus revealing a high exchange activity of ARHGEF18 on RhoA in physiological flow condition that is reduced in pathological shear stress situations (Figure 1D, lane 2 to 4)). As in static condition, $Rac1^{G15A}$ mutant was unable to trap ARHGEF18 in ECs exposed to SS (Figure 1E). Overall, this demonstrates that ARHGEF18 is a RhoGEF specific for RhoA in ECs whose expression and activity are modulated by flow. Though its protein expression is reduced in ECs exposed to physiological SS, its activity is high. In contrast, pathological SS condition presented a higher level of ARHGEF18 protein which is not associated with any gain in activity.

ARHGEF18 is expressed in arterial EC and localizes to tight junction

In epithelial cells, ARHGEF18 has been shown to participate in tight junction formation[41]. We thus assessed the possible interaction of ARHGEF18 with proteins involved in EC junctions. Co-immunoprecipitation of the VE-cadherin complex did not allow the detection of ARHGEF18 in the immunoprecipitated fraction (Fig 1F, left). In contrast, ARHGEF18 was present in the immunoprecipitated fraction of the ZO-1 complex (Fig 1F, right). We next used immunofluorescence staining of retinas from adult mice to verify the expression of ARHGEF18 *in vivo* in the vasculature. Using isolectin B4 staining to label ECs, we identified ARHGEF18 expressed in the arteries of the retina but not in the veins or in the capillaries (Fig 1G). Interestingly the staining was stronger in arteries close to the optic nerve (Fig 1D, artery first order) and fainted as the arteries caliber decreased and as the network ramified to become capillary (Fig suppl 1E). Altogether, these data showed that ARHGEF18 is expressed in arterial EC *in vivo* and localizes to the tight junction by interacting with ZO-1.

ARHGEF18 participates in ECs adhesion and migration

We next assessed the functional role of ARHGEF18 in ECs adhesion and migration, two processes that depend on the dynamic organization of the actin cytoskeleton and the activity of the Rho proteins. We used siRNA silencing and shRNA silencing strategies to turn off the expression of ARHGEF18 protein in ECs. siRNA silencing reduced the expression of ARHGEF18 by 72%(Fig suppl 2A) and shRNAs by 90% with the two shRNAs selected, namely shA18.1 and shA18.4 (Fig suppl 2B). We first evaluated the consequence of ARHGEF18 loss on RhoA activity by pull-down assay using GST-RBD beads. Under physiological SS, RhoA activity was decreased by 30% with both shA18.1 and shA18.4 shRNA expressing ECs (Fig suppl 2C), which was in line with the specificity of ARHGEF18 for RhoA.
We first observed that ARHGEF18 silencing decreased cell-surface interaction analyzed by real-time impedance measurement (Fig 2A and Fig 2D). Both adhesion, corresponding to the linear phase of impedance rise (Fig 2A,B and Fig 2D,E), and spreading of ECs, represented by the maximal value of impedance (Fig 2C and 2F), were decreased. This was observed with siRNA (approximately 25% decrease) as well as with shRNA silencing (approximately 50% decrease). To further characterize this effect at single-cell level, ECs were plated onto fibronectin-coated L-shaped that overcomes the variability in cell morphology by forcing cells to seed individually and to adopt a normalized geometry and allowing a better comparison and quantification of focal adhesion number and size. Both with siRNA (Fig 2G) and with shRNA (Fig 2H) strategies, silencing of ARHGEF18 led to a significant decrease in focal adhesion number compared to control condition (siCTR or shNT respectively). Specifically, the number of focal adhesion site longer than 5um were decreased with both siRNA and shRNA targeting ARHGEF18 compared to their respective control suggesting a defect in focal adhesion maturation.
Basal adhesion as well as maintenance of proper cell-to-cell contact are also a key element in cell migration. Therefore, we investigated if ARHGEF18 would participate in ECs migration. In a wound

healing assay, we observed that the closure of the wound was slowed down in ARHGEF18 silenced ECs compared to control ECs (Fig 2I,J,K) suggesting that ARHGEF18 is involved in collective cell migration. Overall, we identified that ARHGEF18 promotes adhesion, focal adhesion sites formation and migration in ECs *in vitro*.

ARHGEF18 participates in ECs response to flow

As we identified that ARHGEF18 was particularly active when ECs were exposed to physiological SS (Fig 1D) we investigated if ARHGEF18 could contributed to ECs physiological response to flow. First, As expected, control ECs (shNT) aligned and elongated in the direction of flow, harbored continuous VE-cadherin junction with junction-associated lamellipodia formation at the front and rear of the cells, continuous ZO-1 staining as well as cortical actin cables (Fig 3A, upper panel). On the opposite, ECs deficient in ARHGEF18 (shA18.1 and shA18.4) failed to elongate and align in the flow direction under physiological SS(Fig 3B and Fig suppl 3B), leading to a significant decrease in the flow-response index which integrates both the aspect ratio of each cell (major axis length / minor axis lenght) and its angle with the flow direction. Additionally, ARHGEF18 silencing (shRNA strategy) was not affecting the proliferation rate of ECs under PSS, ruling out a possible contribute of proliferation on cell shape in our experimental setting (Fig suppl 3A). VE-cadherin was still present at junctions in ARHGEF18 deficient ECs but the number of gaps in-between cells significantly increased compared to control ECs (Fig 3A, C and Fig suppl 3B). ZO-1 localization at junction appeared disrupted and was significantly decrease compared to control condition (Fig 3A,D; Fig suppl 3B). In the same line, cortical actin was significantly less abundant in ECs deficient in ARHGEF18 compared to control (Fig 3A,E; Fig suppl 3B). As tight junctions are also composed of Claudins, we then assessed the effect of ARHGEF18 loss on Claudin 5 localization, the most abundant Claudin in ECs. To do so, we took advantage of mosaic experiment were the shRNA expression (shA18.1) was not induced in all ECs. Interestingly, we observed that the intensity of the peak of claudin5 at junction (colocalizing with VE-cadherin) in-between a control ECs and an EC expressing the shRNA (GFP tagged) (Fig 3F and 3G middle graph) was decreased compared to the intensity of the peak of claudin5 in-between two control ECs (not expressing the shRNA, Fig 3F and 3G upper graph, Fig suppl 3D). This peak was almost absent in-between two ECs expressing the shRNA (both GFP tagged) (Fig 3F and 3G lower graph, Fig suppl 3D). Additionally, we observed a slight decrease in Claudin 5 expression by western Blot in ECs expressing the shRNA sh18.1 and a significant decrease in ECs expressing the shRNA sh18.4 (Fig suppl 3E) suggesting that loss of ARHGEF18 lead to tight junction destabilization under physiological SS which could affect Claudin 5 protein expression or stability. Finally, as focal adhesions were affected by ARHGEF18 loss under static condition (Fig 2G,H) and as focal adhesion participate in ECs response to SS[24], we analyzed the effect of ARHGEF18 depletion on paxillin expression and localization in ECs exposed to physiological SS. Interestingly, while Paxillin staining revealed that focal adhesion appeared long and mostly collectively oriented in almost all control ECs (classified as paxillin High), ARHGEF18 deficient ECs had less of these “paxillin High” ECs and presented significantly more ECs with short and disorganized focal adhesions (classified as paxillin Low) (Fig 3H, I and Fig suppl 3F,G). Quantification confirmed the significant change in the shape of focal adhesion/paxillin staining induced by ARHGEF18 depletion in EC in PSS condition (Fig 3I and Fig suppl 3G). Surprisingly, this change of paxillin was not associated with modification of paxillin phosphorylation level, assessed by western blot, in ECs deficient in ARHGEF18 compared to control (Fig suppl 3H). Altogether, these data showed that ARHGEF18 contributed to ECs response to physiological SS by promoting tight junction formation and actin recruitment at cell-cell junction and preventing paracellular gaps formation but also by participating in focal adhesion sites organization but without affecting Paxillin phosphorylation.

p38 MAPK mediates ARHGEF18 effects in flow response of ECs

Several intracellular pathways have been shown to control ECs adhesion and tight junction formation as well as ECs migration, among them Akt, p38 MAPK and ERK1/2 activation play a central role in controlling focal adhesion and actin remodeling[44–48]. Additionally, p38 MPAK and ERK1/2 activity can be controlled by RhoGTPases[49,50]. Thus, we explored the possible implication of p38 MAPK, Akt and ERK1/2 in ARHGEF18-mediated effect on ECs. As expected[51], physiological SS increased p38 phosphorylation in ECs exposed to physiological SS (Fig 4A). ARHGEF18 silencing led to a significant decrease in p38 phosphorylation (Fig 4A; Fig suppl 4A). On the contrary, ERK1/2 phosphorylation and Akt phosphorylation levels remained unchanged in ECs deficient in ARHGEF18 compared to control ECs (Fig suppl 4B and suppl 4C respectively). In order to understand if p38 MAPK participated in ARHGEF18-mediated flow response of ECs, we inhibited p38 pharmacologically using SB239063 (100

nM). As previously shown[52], p38 inhibition significantly reduced ECs elongation and orientation in the flow direction under physiological SS (Fig 4B) thus mimicking ARHGEF18 silencing. We then investigated the effect of p38 inhibition on tight junction and focal adhesion formation induced by physiological SS. As observed in ARHGEF18-depleted EC, p38 MAPK inhibition significantly decreased the amount of ZO-1 at tight junctions, which appeared discontinuous (Fig 4C,D), and slightly but significantly reduced the amount of actin at cell junction (Fig 4 D,E). Surprisingly, these effects were not accompanied with increased gaps number in-between ECs suggesting that part of the effect of ARHGEF18 on EC junctions were not mediated by p38. Paxillin staining also revealed that p38 MAPK inhibition under physiological SS led to the loss of focal adhesion organization similar to that observed with ARHGEF18 silencing (Fig 4F,G). These data suggest that ARHGEF18 participate to EC elongation and alignment in response to PSS by controlling tight junction and focal adhesion via the activation of p38 MAPK.

GEF activity of ARHGEF18 is important for p38 activation and flow response of ECs

To dig further into the mechanism of action of ARHGEF18, we wanted to define whether its role in p38 activation and EC response to PSS was due to its ability to induce guanine nucleotide exchange on Rho proteins. We thus generated ECs over-expressing the Y260A-ARHGEF18 inactive mutant (FlAG tagged) that has no guanine nucleotide exchange factor activity[39], These ECs also expressed shRNA targeting the endogenous form of ARHGEF18 to eliminate potential effects due endogenous ARHGEF18 activity. We validated our constructs, by checking in a pull-down assay the inability of the Y260A-ARHGEF18 mutant to interact with the nucleotide free RhoA ($RhoA^{G17A}$), while the WT-ARHGEF18 generated a strong interaction (Fig 5A). Under physiological SS, p38 MAPK phosphorylation was reduced in Y260A-ARHGEF18 expressing ECs compared to ECs over-expressing the WT form (Fig 5B). This effect was associated with a failure of Y260A-ARHGEF18 expressing ECs to elongate and align in the direction of the flow while ECs expressing the WT form elongated and aligned properly in response to physiological SS (Fig 5C and D). Additionally, no gaps were observed in ECs monolayer expressing either the WT or GEF mutant ARHGEF18 under physiological SS, confirming that ARHGEF18 must have another function to regulate gap formation. To assess the involvement of the GEF activity of ARHGEF18 in tight junction formation, we took advantage of mosaic experiment were the Y260A-ARHGEF18 inactive mutant was not expressed in all ECs. In those experiment, examination of tight junction by ZO-1 staining show a strong peak of ZO-1, colocalized with VE-cadherin at junction in-between two control ECs (Fig 5E and 5F left graph), which was decreased at the junction in-between a WT EC and a Y260A-ARHGEF18 expressing EC (Fig 5E and 5F middle graph) and almost absent at the junction of two Y260A-ARHGEF18 expressing ECs (Fig 5E and 5F right graph). We also observed that the intracellular staining of ZO-1 was increased in Y260A-ARHGEF18 expressing EC compared to control ECs (Fig 5E and F). In these experiments, we also observed a slight decrease in VE-cadherin staining intensity in-between control and GEF-mutant ECs or in-between 2 GEF-mutant ECs, something we did not observed with ARHGEF18 silencing. Lastly, in ECs with low and local over-expression of the GEF-mutant, we observe a focal loss of ZO-1 together with a dissolution of the VE-cadherin junction (Fig 5E, lower panel). Overall, these data highlight the requirement of the nucleotide exchange activity of ARHGEF18 for the activation of p38 MAPK and the subsequent EC response to physiological flow.

Discussion

Our present work identifies a new SS-sensitive RhoGEF in ECs: ARHGEF18. ARHGEF18, also known as p114-RhoGEF, has been described mostly in epithelial cells where it controls cell tight junction maturation and apicobasal polarity establishment[39,53] via RhoA and Rac1 activation[54–56]. At the junction of epithelial cells, ARHGEF18 is shown to localized at tight junctions where it regulates RhoA-Rock activity and actomyosin contractility in spatio-temporal manner[39]. ARHGEF18 has also been shown to participate in long range communication of epithelial cell to pass the pulling force information from leading cells to neighboring cells in a wound closure assay, suggesting a potential mechano-sensitive role of this protein[41]. In this work, focusing on endothelial cells, we showed that ARHGEF18 expression and activity is modulated by the magnitude of SS applied. Interestingly, ARHGEF18 activity is at its highest when ECs are exposed to physiological SS suggesting a beneficial role of this Rho-GEF on ECs biology. This high activity is associated with a lower expression of the protein than in pathological SS, suggesting the failure in ARHGEF18 activation by pathological SS leads to its over-expression. Data from epithelial cells and GTP transfer experiments were in favor of a specificity of ARHGEF18 for the

RhoGTPase RhoA[54]. In ECs, we also demonstrated this specificity for RhoA, as ARHGEF18 was unable to bind to Rac1 in any SS condition. ARHGEF18 is not the only RhoGEF able to activate RhoA in ECs, therefore the effect at the total cellular level, as assessed by pulldown, could have been missed. The observation of a reduction of RhoA activity in total cell lysat is thus strongly in favor of an essential role of ARHGEF18 in the SS-induced activation of RhoA in ECs. From works done in epithelial cells, it appears that ARHGEF18 can localize to both adherent and tight junction, being recruited there by Gα12 or JAM-A respectively[58,59]. The only other article studying ARHGEF18 in ECs showed ARHGEF18 recruitment to tight junction of dermal microvascular ECs by both ZO-1 and JACOP[60]. In both cell type, this localization of ARHGEF18 was responsible for establishing cell tension at junction. None of these studies showed a direct interaction between ARHGEF18 and those junctional proteins. Unfortunately, we were unable to stain for ARHGEF18 *in vitro* in ECs, and could not observe ARHGEF18 at junctions in ECs nor evaluate the influence of SS on this localization. However, we successfully co-precipitated ARHGEF18 and ZO-1, showing the direct interaction of these 2 proteins in ECs implying the junctional localization of ARHGEF18. Interestingly, in ECs, ARHGEF18 is not interacting with VE-Cadherin, suggesting that ARHGEF18 does not directly impact adherent junctions. Our data from the over-expression of the Y260A-ARHGEF18 mutant showed a trapping of ZO-1 within the cytoplasm in mutant cells, suggesting that in opposition to what has been shown in microvascular ECs under static condition where ZO-1 acts upstream to ARHGEF18 bringing it to tight junctions, ARHGEF18 would participate in ZO-1 localization to tight junction in ECs under physiological SS. Additionally, we successfully stained the vasculature of the retina in mice, showing that ARHGEF18 was indeed expressed in ECs *in vivo*, but also that it expression correlates with arterial specification, ie. strongly expressed in more mature arteries (close to the optic nerve) and weakly expressed in less mature arteries (distant from the optic nerve). This observation could mean either a role of arterial specification in ARHGEF18 expression or a role of SS as arteries from different caliber are exposed to different SS level. In epithelial cell, ARHGEF18 contribution to cell-cell tension[39] and long range communication[41] participates in cell adhesion and collective migration. In our hands, migration and adhesion were also affected in ARHGEF18-silenced ECs, suggesting that similar mechanisms could be at play. Whether it goes through similar effectors as the one identified in epithelial cell, namely Patj, LKB1 and Lulu2 is still to determined.

In ECs, cell-cell tension participates in SS sensing allowing collective behavior[61]. Interestingly ARHGEF18 silencing leads to a loss of ECs alignment in response to physiological SS, a hallmark of endothelial health and collective behavior. This is accompanied by a loss of the tight junction proteins (ZO-1 and Claudin5) at junctions and a destabilization of cortical actin. This is the first observation showing that a RhoA-specific RhoGEF can control EC response to flow. Interestingly, loss of ARHGEF18 not only disrupts tight junction under physiological SS but also impairs focal adhesion formation and organization, suggesting a cross-talk between tight junction and focal adhesion. We also observed a loss in focal adhesion in single cell adhesion experiment suggesting a direct role of ARHGEF18 on focal adhesion. In dermal microvascular ECs, ARHGEF18 participate in the maintenance of junctional vinculin[60]. As vinculin has been shown as a key element to balance tension between focal adhesions and adherens junctions[62], it would be interesting to evaluate if ARHGEF18 can participate in vinculin localization at focal adhesion or tight junctions and therefore promote their stability. Among the different signaling pathways tested, only p38 MAPK seems to participate in the effect of ARHGEF18 as ARHGEF18 silencing reduces p38 MAPK phosphorylation level and inhibiting p38 MAPK activity reproduces most of the effect of ARHGEF18 silencing. The only effect that was not seen with p38 MAPK inhibition but observed with ARHGEF18 silencing was the formation of paracellular gaps, suggesting that ARHGEF18 downstream signaling does not fully depend on p38 MAPK. RhoGEF proteins not only carry GEF activity but usually display additional roles depending on their structure. As an example, Trio has been shown in ECs to contribute to Rac1 localization within the cell but not to Rac1 activity while having a GEF domain specific for Rac1[35]. In our hands, nucleotide exchange activity of ARHGEF18 contributes to tight junction formation as ZO-1 mis-localizes from junctions in Y260A-ARHGEF18 expressing ECs. In the same line as p38 MAPK inhibition, the Y260A mutation does not trigger paracellular gaps, suggesting once more an additional role of ARHGEF18 independent of its nucleotide exchange activity. Interestingly, in mice, complete deletion of ARHGEF18 resulted in embryonic lethality[63]. ARHGEF18 null embryos showed reduced vasculature, increased hemorrhage and oedema, which is in line with our *in vitro* observation. Future work will aim at better understanding the specific role of ARHGEF18 in endothelial cell *in vivo* both in physiology and pathologies.

Acknowledgments
We thank Dr. Vincent Sauzeau and Dr. Thibaut Quillard for helpful comments on the manuscript. We are most grateful to the Genomics Core Facility GenoA, member of Biogenouest and France Genomique and to the Bioinformatics Core Facility BiRD, member of Biogenouest and Institut Français de Bioinformatique (IFB) (ANR-11-INBS-0013) for the use of their resources and their technical support. We acknowledge the IBISA MicroPICell facility (Biogenouest), member of the national infrastructure France-Bioimaging supported by the French national research agency (ANR-10-INBS-04). This work was supported by the NeXT initiative (A.-C. Vion, S. Batta and C. Lebot), the French national research agency (ANR) (A.-C. Vion) and the local fund Genavie (S. Batta). The authors declare no competing financial interests. Author contributions: S. Batta performed experiments, analyzed the results, and wrote the manuscript. M. Rio, C. Lebot, C. Baron-Menguy performed experiments and analyzed results, R. Leruz performed experiments. G Loirand reviewed the manuscript. A.-C. Vion designed the study, performed experiments, analyzed the results, and wrote the manuscript.

Tables

Table 1: shRNA sequences used in this study

Name	Sense (5'->3')	Antisense (5'->3')	Target
shNT (non-target)	CAAATCACAGAATCGTCGTAT	ATACGACGATTCTGTGATTTG	None
shArhgef18.1	GGCCACAATGAAGCTGTTAGT	ACTAACAGCTTCATTGTGGCC	Exon
shArhgef18.2	CAAAACTTGATCAAGAAAATT	AATTTTCTTGATCAAGTTTTG	Exon
shArhgef18.3	CGGGCTACGACTGCACAAACA	TGTTTGTGCAGTCGTAGCCCG	Exon
shArhgef18.4	AAGACAAGATGTCCTTTATGA	TCATAAAGGACATCTTGTCTT	Exon
shArhgef18.5	CGATTTTATTTGTAAAGTTGA	TCAACTTTACAAATAAAATCG	3'UTR
shArhgef18.6	GAGCAAATGTTCCTATTTTCG	CGAAAATAGGAACATTTGCTC	3'UTR

Table 2: Primers and oligos used to amplify Arhgef18

Oligo name	Oligo sequence (5'->3')
Arhgef18_Fw	ACAGCTCTGCGATCGCCACCATGACGGTCTCTCAGAAAGGG
Arhgef18_Rev	GCTGTCTCGAGAATTAAGAAGAAGATGACGTCTTCTTTGC
ORF18-Oligo1	ATGACGGTCTCTCAGAAAGGG
ORF18-Oligo2	GTACGTCGGTCAGCAGGATAG
ORF18-Oligo3	CTCACCTTCCGCAAGGAAGAC
ORF18-Oligo4	GAAGTTGCGTTGCCGCTCCTG
ORF18-Oligo5	CCCACCAGGACAGCTATGTG
ORF18-Oligo6	GAAGAAGATGACGTCTTCTTTGCTGG

Figure 1

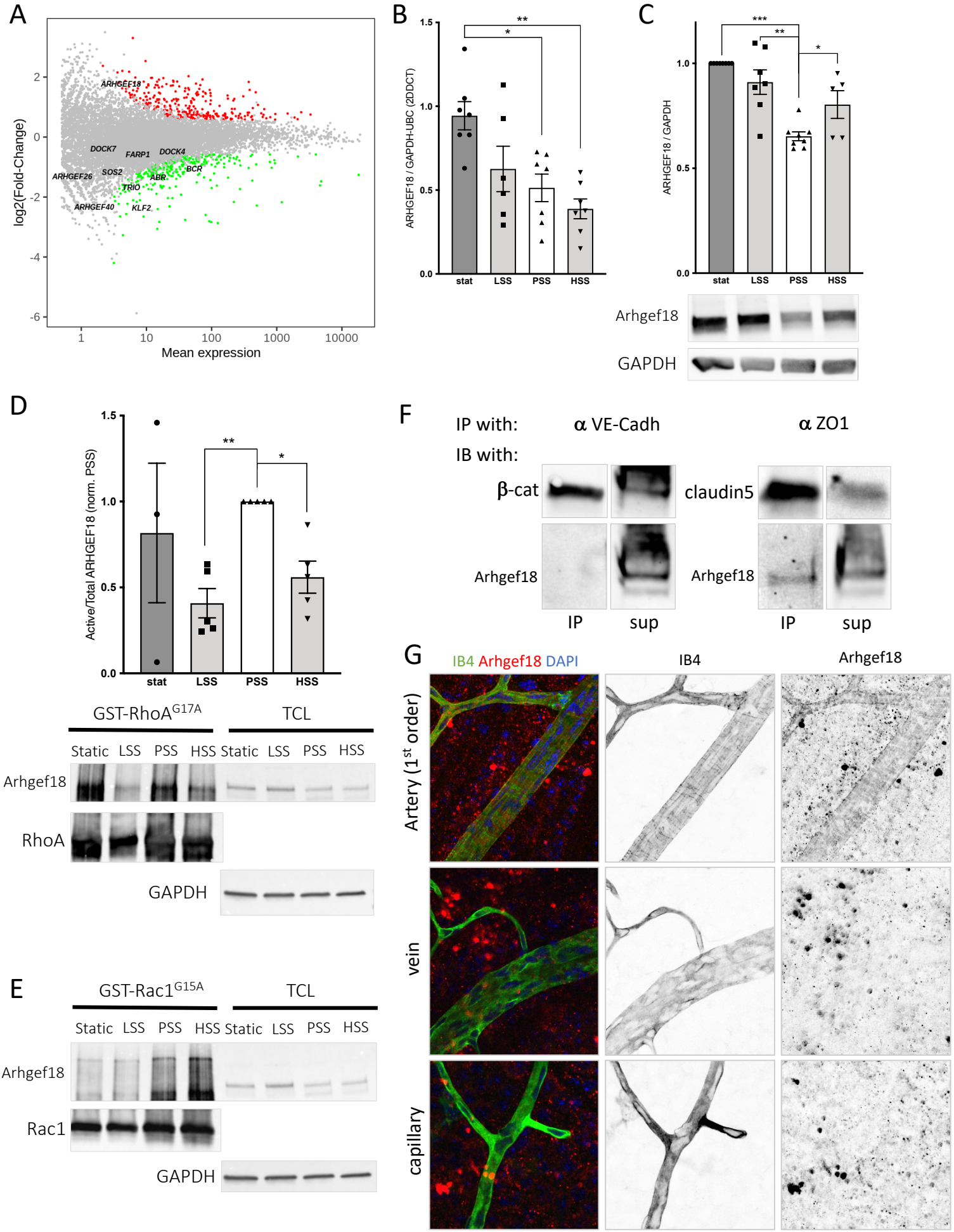
A
log2(Fold-Change)
Mean expression
ARHGEF18
DOCK7
FARP1
DOCK4
ARHGEF26
SOS2
ABR
BCR
TRIO
ARHGEF40
KLF2
B
ARHGEF18 / GAPDH-UBC (2DDCT)
stat
LSS
PSS
HSS
C
ARHGEF18 / GAPDH
Arhgef18
GAPDH
D
Active/Total ARHGEF18 (norm. PSS)
GST-RhoA^{G17A}
TCL
Static LSS PSS HSS Static LSS PSS HSS
Arhgef18
RhoA
GAPDH
E
GST-Rac1^{G15A}
TCL
Static LSS PSS HSS Static LSS PSS HSS
Arhgef18
Rac1
GAPDH
F
IP with:
α VE-Cadh
α ZO1
IB with:
β-cat
claudin5
Arhgef18
Arhgef18
IP
sup
IP
sup
G
IB4 Arhgef18 DAPI
IB4
Arhgef18
Artery (1st order)
vein
capillary

Figure 2

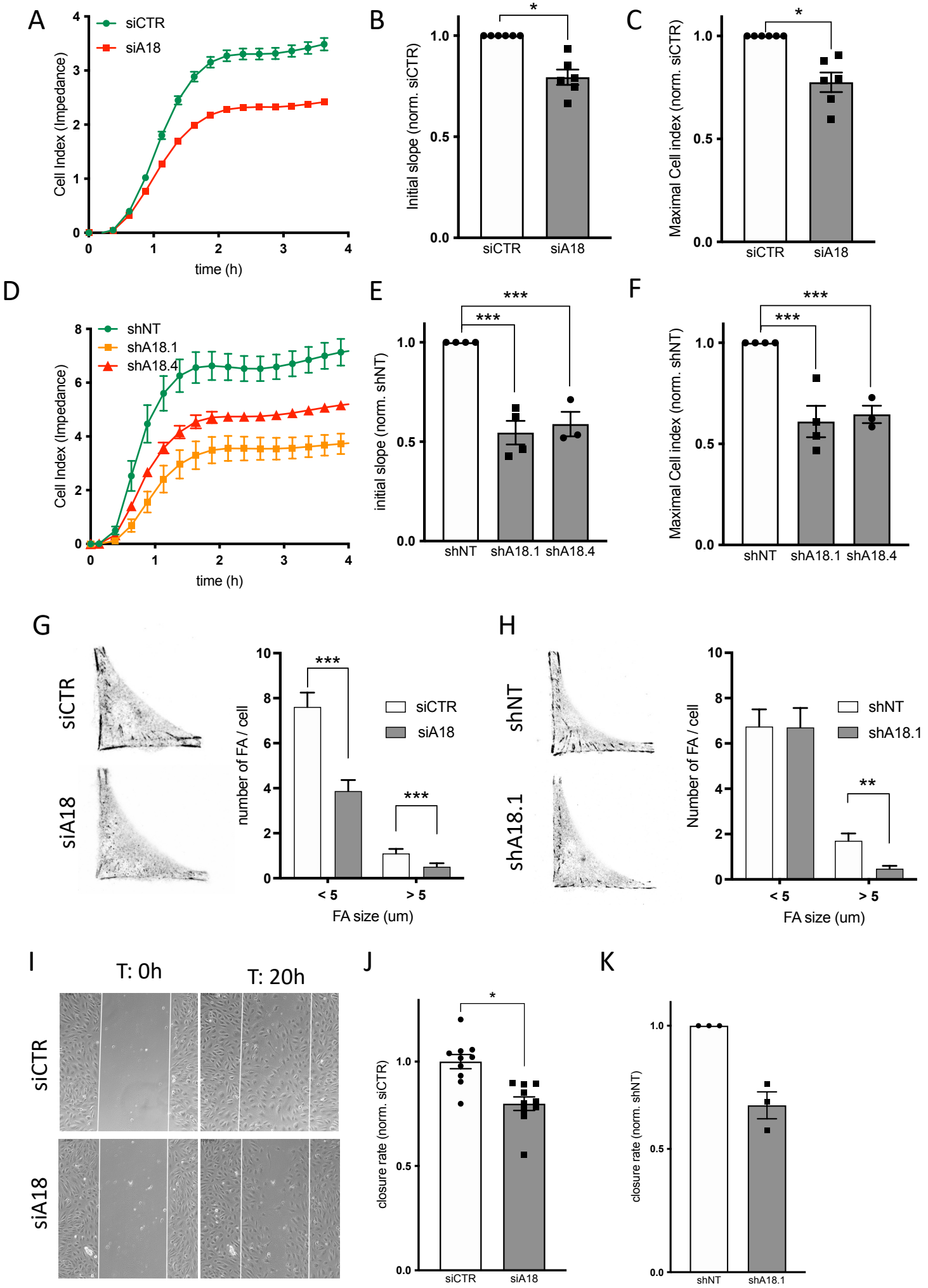
A
siCTR
siA18
Cell Index (Impedance)
time (h)
B
Initial slope (norm. siCTR)
siCTR
siA18
C
Maximal Cell index (norm. siCTR)
D
shNT
shA18.1
shA18.4
E
initial slope (norm. shNT)
F
Maximal Cell index (norm. shNT)
G
siCTR
siA18
number of FA / cell
FA size (um)
H
shNT
shA18.1
Number of FA / cell
I
T: 0h
T: 20h
J
closure rate (norm. siCTR)
K
closure rate (norm. shNT)

Figure 3

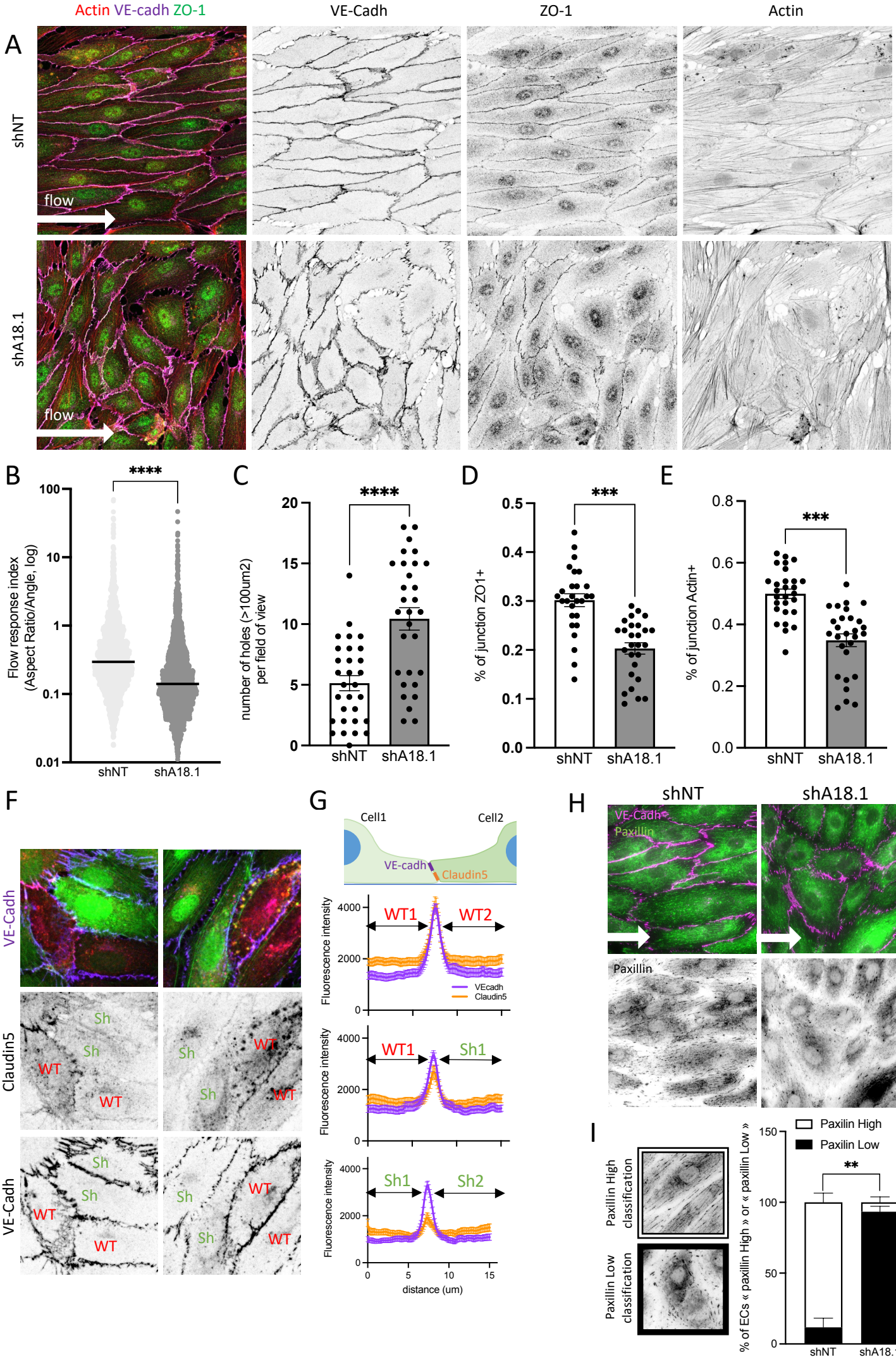
Actin VE-cadh ZO-1
VE-Cadh
ZO-1
Actin
A
shNT
shA18.1
flow
flow
B
****
Flow response index (Aspect Ratio/Angle, log)
100
10
1
0.1
0.01
shNT
shA18.1
C
****
number of holes (>100um2) per field of view
20
15
10
5
0
shNT
shA18.1
D
***
% of junction ZO1+
0.5
0.4
0.3
0.2
0.1
0.0
shNT
shA18.1
E
***
% of junction Actin+
0.8
0.6
0.4
0.2
0.0
shNT
shA18.1
F
GFP Claudin5 VE-Cadh
Claudin5
VE-Cadh
Sh
WT
G
Cell1
Cell2
VE-cadh
Claudin5
Fluorescence intensity
4000
2000
0
WT1
WT2
VEcadh
Claudin5
WT1
Sh1
Sh1
Sh2
0
5
10
15
distance (um)
H
shNT
shA18.1
VE-Cadh
Paxillin
Paxillin
I
Paxillin High classification
Paxillin Low classification
Paxilin High
Paxilin Low
**
% of ECs « paxillin High » or « paxillin Low »
150
100
50
0
shNT
shA18.1

Figure 4

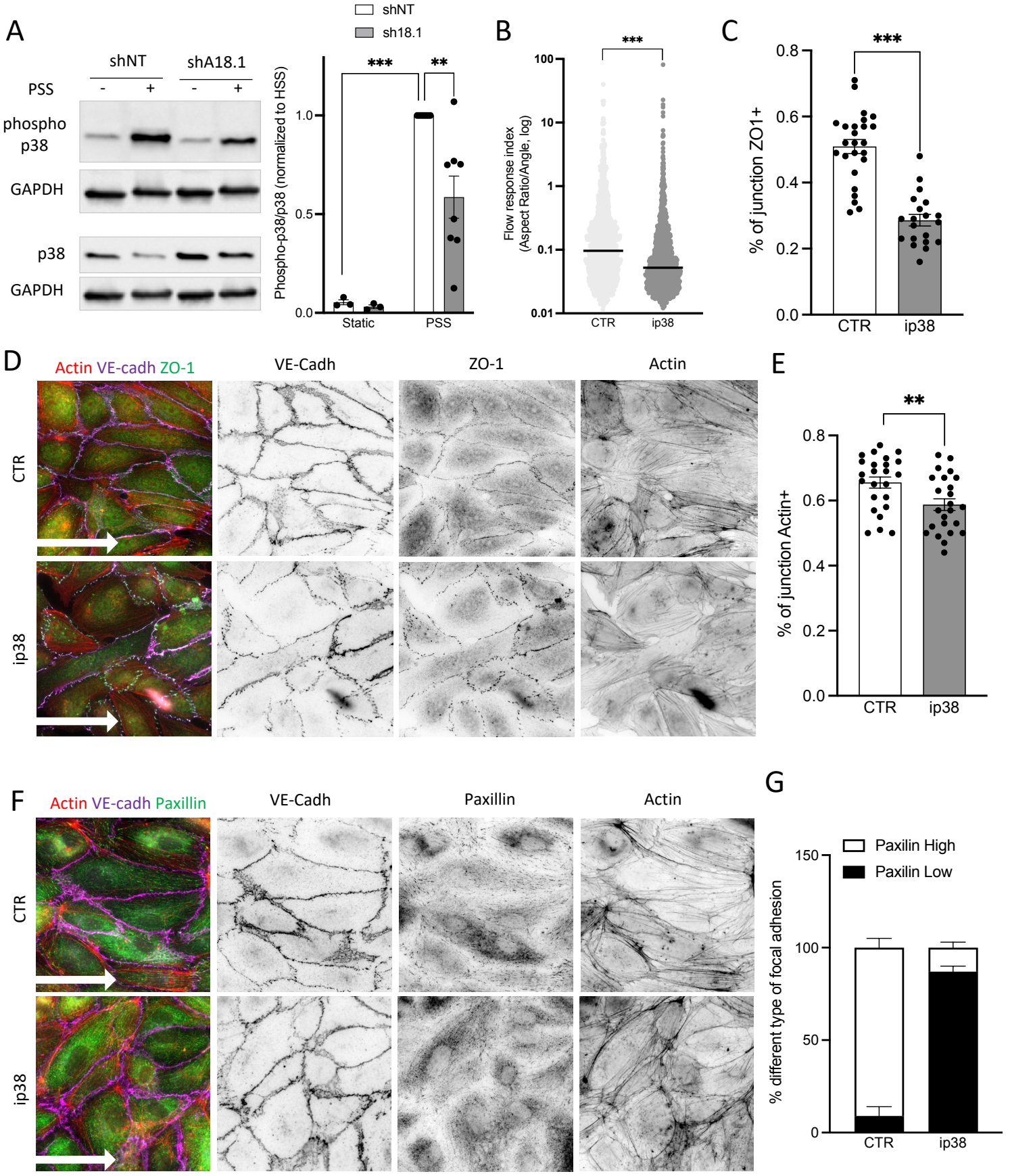
A
shNT
shA18.1
PSS
- + - +
phospho p38
GAPDH
p38
GAPDH
shNT
sh18.1
Phospho-p38/p38 (normalized to HSS)
***
**
Static
PSS
B
***
Flow response index (Aspect Ratio/Angle, log)
CTR
ip38
C
***
% of junction ZO1+
CTR
ip38
D
Actin VE-cadh ZO-1
VE-Cadh
ZO-1
Actin
CTR
ip38
E
**
% of junction Actin+
CTR
ip38
F
Actin VE-cadh Paxillin
VE-Cadh
Paxillin
Actin
CTR
ip38
G
Paxilin High
Paxilin Low
% different type of focal adhesion
CTR
ip38

Figure 5

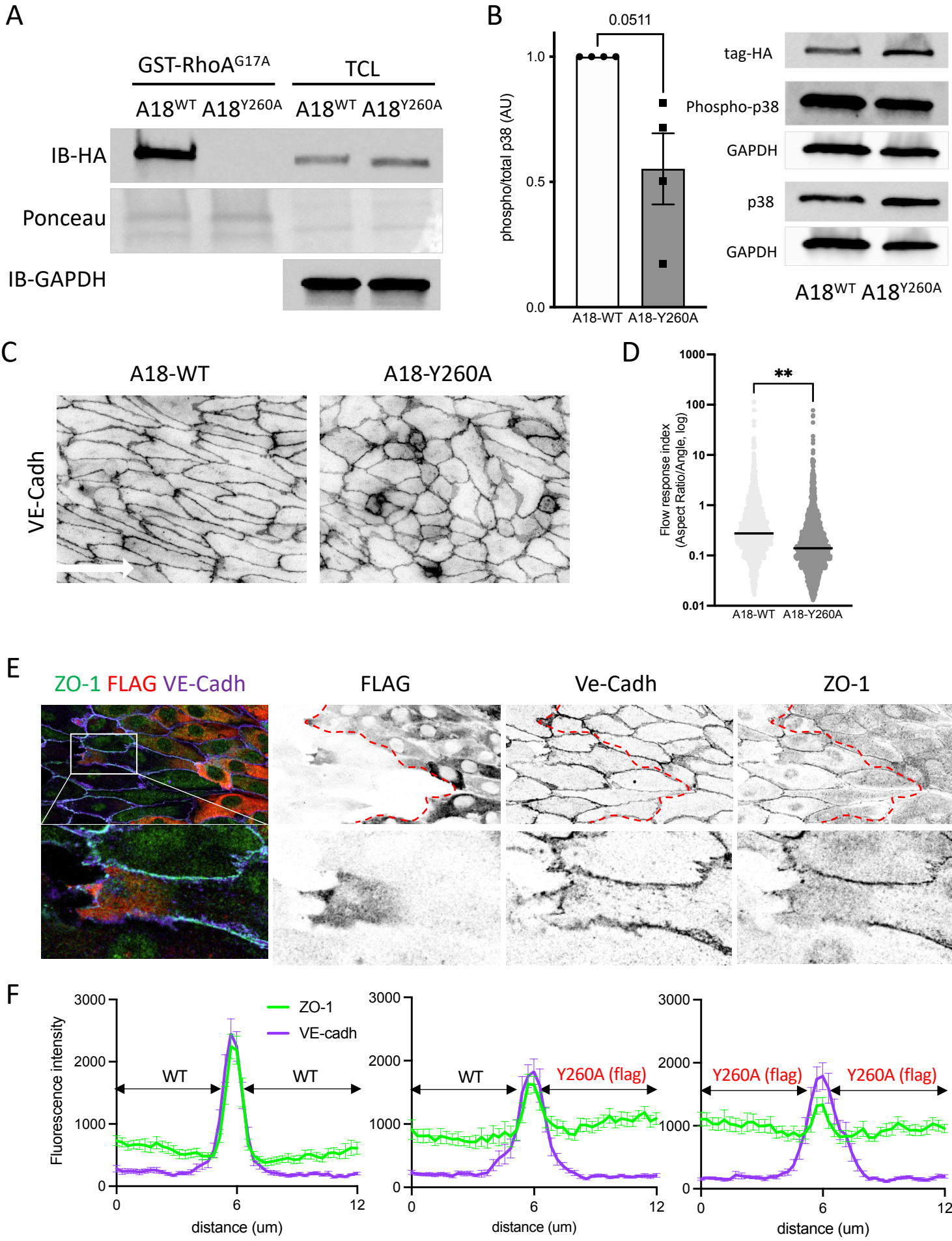
A
GST-RhoA^G17A
TCL
A18^WT A18^Y260A
A18^WT A18^Y260A
IB-HA
Ponceau
IB-GAPDH
B
0.0511
phospho/total p38 (AU)
1.0
0.5
0.0
A18-WT A18-Y260A
tag-HA
Phospho-p38
GAPDH
p38
GAPDH
A18^WT A18^Y260A
C
A18-WT
A18-Y260A
VE-Cadh
D
**
Flow response index
(Aspect Ratio/Angle, log)
1000
100
10
1
0.1
0.01
A18-WT A18-Y260A
E
ZO-1 FLAG VE-Cadh
FLAG
Ve-Cadh
ZO-1
F
Fluorescence intensity
3000
2000
1000
0
ZO-1
VE-cadh
WT
WT
WT
Y260A (flag)
Y260A (flag)
Y260A (flag)
0
6
12
distance (um)

Figures Legends

Figure 1: ARHGEF18 expression and activity is shear-stress dependent and bound to RhoA but not RAC1. **A.** MA plot comparing gene expression between static condition and high shear stress. 24h of SS. Green dots: up-regulated genes in HSS condition; red dots: down-regulated genes in HSS condition. N=4. **B.** qPCR analysis of Arhgef18 RNA expression level. 24h of SS, LSS: low shear stress; PSS: physiological shear stress; HSS: high shear stress. N>5. *p<0.05; **p<0.01; One-way ANOVA. **C.** Western-Blot analysis of ARHGEF18 protein expression level (left, quantification; right, representative blot). 24h of SS, LSS: low shear stress; PSS: physiological shear stress; HSS: high shear stress. N>5. *p<0.05; **p<0.01; ***p<0.001; One-way ANOVA. **D.** Quantification and representative blot of ARHGEF18 binding on nucleotide-free RhoA (GST-RhoA^{G17A}) by pull-down assay. 24h of SS, LSS: low shear stress; PSS: physiological shear stress; HSS: high shear stress. N=5. *p<0.05; **p<0.01; ***p<0.001; One-way ANOVA. **E.** Representative blot of ARHGEF18 binding on nucleotide-free Rac1 (GST-Rac1^{G15A}) by pull-down assay. 24h of SS, LSS: low shear stress; PSS: physiological shear stress; HSS: high shear stress. Representative of N=3. **F.** Representative blot from Co-immunoprecipitation of ARHGEF18 with VE-cadherin (left) or ZO-1 (right). Co-immunoprecipitation efficiency was assessed by the presence of β-catenin and Claudin 5 in the immunoprecipitated fraction of VE-cadherin complex and ZO-1 complex respectively (upper lanes). Static condition. Representative of N=2. **G.** Immunofluorescent staining of ARHGEF18 in mouse retina. Retinas from 4 weeks-old animals. Green: Isolectin B4; Representative of N=5.

Figure 2: ARHGEF18 participates to endothelial cell adhesion and migration. A. Representative curves of impedance measurement during adhesion of HUVECs. Green: non-targeting siRNA (siCTR); red: siRNA targeting arhegf18 RNA (siA18). . **B.** Quantification of adhesion speed (slope of the linear part of the curve) of HUVECs transfected with a control siRNA (siCTR) or with an siRNA targeting Arhgef18 (siA18). N=6. *p<0.05; Wilcoxon T-test. **C.** Quantification of maximal adhesion (plateau of the curve) of HUVECs transfected with a control siRNA (siCTR) or with an siRNA targeting Arhgef18 (siA18). N=6. *p<0.05; Wilcoxon T-test. **D.** Representative curves of impedance measurement during adhesion of HUVECs. Green: non-targeting shRNA (shNT); red and orange: shRNAs targeting arhgef18 RNA (shA18.4 andshA18.1 respectively). **E.** Quantification of adhesion speed (slope of the linear part of the curve) of HUVECs expressing a non-targeting shRNA (shNT) or a shRNA targeting Arhgef18 (shA18.1 or A18.4). N<3. ***p<0.001; One-way ANOVA. **F.** Quantification of maximal adhesion (plateau of the curve) of HUVECs expressing a non-targeting shRNA (shNT) or a shRNA targeting Arhgef18 (shA18.1 or A18.4). N<3. ***p<0.001; One-way ANOVA. **G.** Representative images of HUVECs adhesion on L-shaped micropattern immune-stained for paxillin (siRNA transfected HUVECs) and Quantification of focal adhesion number and size. N=39 (cells) from 4 different experiments. ***p<0.001; 2-way ANOVA. **H.** Representative images of HUVECs adhesion on L-shaped micropattern immune-stained for paxillin. (shRNA expressing HUVECs) and Quantification of focal adhesion number and size. N=51 (cells) from 4 different experiments. ***p<0.001; 2-way ANOVA. **I.** Representative images of wound assay experiment (phase contrast images) at starting point (T:0h) and 20h post wound. siRNA transfected HUVECs. **J.** Quantification of closure speed of HUVECs transfected with a control siRNA (siCTR) or with an siRNA targeting Arhgef18 (siA18). N=10. *p<0.05; paired T-test. **K.** Quantification of closure speed of HUVECs expressing a control shRNA (shNT) or a shRNA targeting Arhgef18 (shA18.1). N=3.

Figure 3: ARHGEF18 participates in ECs response to flow, tight junction formation and focal adhesion formation. A. Representative images of HUVECs expressing a non-targeting shRNA (shNT) or a shRNA targeting Arhgef18 (shA18.1), exposed to physiological SS and stained for ZO-1 (green), VE-cadherin (magenta) and actin (red). Flow direction is indicated by the arrow. **B.** Quantification of cell orientation and elongation with the flow in HUVECs expressing a non-targeting shRNA (shNT) or a shRNA targeting Arhgef18 (shA18.1), exposed to physiological SS. 24h of SS. Each dot represents a cell. N=5 with in-between 200 and 600 cells analyzed by experiment. ***p<0.001; Mann-Whithney T-test. **C.** Quantification of number of holes in-between cells in HUVECs expressing a non-targeting shRNA (shNT) or a shRNA targeting Arhgef18 (shA18.1), exposed to physiological SS. 24h of SS. N=3, 10 areas analyzed by experiment. ***p<0.001; Unpaired T-test. **D.** Quantification of ZO-1 localized at junction in HUVECs expressing a non-targeting shRNA (shNT) or a shRNA targeting Arhgef18 (shA18.1), exposed to physiological SS. 24h of SS. N=3, 9 areas analyzed by experiment. ***p<0.001; Unpaired T-test. **E.** Quantification of Actin localized at junction in HUVECs expressing a non-targeting shRNA (shNT) or a shRNA targeting Arhgef18 (shA18.1), exposed to physiological SS. 24h of SS. N=3, 9 areas analyzed by experiment. ***p<0.001; Unpaired T-test. **F.** Representative images of Claudin5 staining in a mix population of WT cells (GFP negative, non-green, indicated as “WT” on images) and cells expressing a shRNA targeting Arhgef18 (shA18.1, GFP positive, green, indicated as “KO” on images), exposed to physiological SS. Green: GFP; red: Claudin5; Magenta: VE-cadherin. **G.** Quantification of the Claudin5 staining at junction using plot profile analysis. N=3, 12 couple of cells analyzed per experiment. **H.** Representative images of Paxillin staining in HUVECs expressing a non-targeting shRNA (shNT) or a shRNA targeting Arhgef18 (shA18.1), exposed to physiological SS. Flow direction is indicated by the arrow. Green: paxillin; magenta: VE-cadherin. **I.** Quantification of focal adhesion type by hand classification of paxillin staining within each cell based on the representative images for each category on the left (white box: paxillin high = numerous, elongated and aligned focal adhesions; black box: paxillin low = few, short and misaligned focal adhesions). N=4. Quantified blindly.

Figure 4: p38 mediates ARHGEF18 effects in flow response of ECs. A. Quantification of p38 phosphorylation by Western blot in HUVECs expressing a non-targeting shRNA (shNT) or a shRNA targeting Arhgef18 (shA18.1), under static condition or exposed to physiological SS (PSS). Static: N=3; PSS: N=8. **p<0.01; ***p<0.001 2-way ANOVA**. B.** Quantification of cell orientation and elongation with the flow in HUVECs treated with an inhibitor for p38 (SB239063, 100nM, ip38) or vehicle (CTR), exposed to physiological SS. 24h of SS. Each dot represents a cell. N=4 with in-between 200 and 450 cells analyzed by experiment. ***p<0.001; Mann-Whitney T-test. **C.** Quantification of Actin localized at junction in HUVECs treated with an inhibitor for p38 (SB239063, 100nM, ip38) or vehicle (CTR), exposed to physiological SS. 24h of SS. N=2, 10 to 14 areas analyzed by experiment. **p<0.01; Unpaired T-test. **D.** Representative images of HUVECs treated with an inhibitor for p38 (SB239063, 100nM, ip38) or vehicle (CTR) exposed to physiological SS. 24 and stained for ZO-1 (green), VE-cadherin (magenta) and actin (red). Flow direction is indicated by the arrow. **E.** Quantification of ZO-1 localized at junction in HUVECs treated with an inhibitor for p38 (SB239063, 100nM, ip38) or vehicle (CTR) exposed to physiological SS. 24h of SS. N=2, 10 to 15 areas analyzed by experiment. ***p<0.001; Unpaired T-test. **F.** Representative images of Paxillin staining in HUVECs treated with an inhibitor for p38 (SB239063, 100nM, ip38) or vehicle (CTR), exposed to physiological SS. Flow direction is indicated by the arrow. Green: paxillin; magenta: VE-cadherin; red: Actin. **G.** Quantification of focal adhesion type by hand classification of paxillin staining within each cell based on the representative images for each category on the left (white box: paxillin high = numerous, elongated and aligned focal adhesions; black box: paxillin low = few, short and misaligned focal adhesions). N=2. Quantified blindly.

Figure 5: GEF activity of ARHGEF18 is important for p38 activation and flow response of ECs. A. Representative blot of ARHGEF18 binding on nucleotide-free RhoA (GST-RhoA^{G17A}) by pull-down assay with HUVECs exposed to physiological SS, over-expressing WT form (A18^{WT}) or mutant form (A18^{Y260A}) of ARHGEF18. **B.** Quantification of p38 phosphorylation by Western blot in HUVECs exposed to physiological SS, over-expressing WT form (A18^{WT}) or mutant form (A18^{Y260A}) of ARHGEF18. N=4. Paired T-test. **C.** Representative images of HUVECs HUVECs exposed to physiological SS, over-expressing WT form (A18^{WT}) or mutant form (A18^{Y260A}) of ARHGEF18 and stained VE-cadherin. Flow direction is indicated by the arrow**. D.** Quantification of cell orientation and elongation with the flow in HUVECs exposed to physiological SS, over-expressing WT form (A18^{WT}) or mutant form (A18^{Y260A}) of ARHGEF18. Each dot represents a cell. N=1 with in-between 1000 and 1350 cells analyzed by experiment. **p<0.01; Unpaired T-test. E. Representative images of ZO-1 staining in a mix population of WT cells (FLAG negative, non-red) and cells over-expressing the mutant form (A18^{Y260A}) of ARHGEF18 (FLAG positive, red), exposed to physiological SS. Green: ZO-1; red: FLAG; Magenta: VE-cadherin. F. Quantification of the ZO-1 staining at junction using plot profile analysis. N=1, 25 couples of cells analyzed per experiment.

Material and Methods

Cell culture and microfluidic chamber experiments

HUVECs (passage 2 to 6; PromoCell) were routinely cultured in EBM media supplemented with the provided growth factors kit (Promocell). For flow experiments dedicated to Pull-down/Co-IP/WB lysate collection, cells were cultured on 0.2% gelatin-coated slides (Menzel Glazer) and unidirectional laminar shear stress was applied using peristaltic pumps (Gilson) connected to a glass reservoir (ELLIPSE) and the chamber containing the slide. For flow experiments dedicated immunofluorescence staining, cells were cultured on 0.2% gelatin-coated 0.4 ibidi slides (IBIDI) and unidirectional laminar shear stress was applied using the pumping system and control unit form IBIDI. Local shear stress was calculated using Poiseuille's law and averaged to 3.6 dyn/cm^2 (pathological low shear stress: LSS) 16 dyn/cm^2 (physiological shear stress: PSS) or 36 dyn/cm^2 (pathological high shear stress: HSS). For p38 MAPK inhibition studies, confluent HUVEC were pretreated with p38 MAPK specific inhibitor (100nM, SB239063; TOCRIS) for at least 1hr prior to physiological SS, treatment was maintained during the flow stimulation.

Mice

Retinas from Wild Type C57/BL6 mice were collected on euthanized mice at 4-week-old in PFA 4% and used for immunofluorescent staining.

3'Sequencing RNA Profiling:

Experimental protocol: The protocol was performed according to the 3′-digital gene expression (3′-DGE) approach developed by the Broad institute as described in https://doi.org/10.21203/rs.3.pex-1336/v1. The libraries were prepared from 10 ng of total RNA in 4µl. The mRNA poly(A) tails were tagged with universal adapters, well-specific barcodes and unique molecular identifiers (UMIs) during template-switching reverse transcription. Barcoded cDNAs from multiple samples were then pooled, amplified and tagmented using a transposon-fragmentation approach which enriches for 3'ends of cDNA : 200ng of full-length cDNAs were used as input to the Nextera™ DNA Flex Library Prep kit (ref #20018704, Illumina) and Nextera™ DNA CD Indexes (24 Indexes, 24 Samples) (ref #20018707, Illumina) according to the manufacturer's protocol (Nextera DNA Flex Library Document, ref #1000000025416 v04, Illumina).

Size library was controlled on 2200 Tape Station Sytem (Agilent Technologies). A library of 350-800 bp length was run on a NovaSeq 6000 using NovaSeq 6000 SP Reagent Kit 100 cycles (ref #20027464, Illumina) with 17*-8-105* cycles reads.

Bioinformatics protocol: Raw fastq pairs match the following criteria: the 16 bases of the first read correspond to 6 bases for a designed sample-specific barcode and 10 bases for a unique molecular identifier (UMI). The second read (104 bases) corresponded to the captured poly(A) RNAs sequence.

Bioinformatics steps were performed using a snakemake pipeline (https://bio.tools/3SRP). Samples demultiplexing was performed with a python script. Raw paired-end fastq files were transformed into a single-end fastq file for each sample. Alignment on refseq reference transcriptome, available from the UCSC download site, was performed using bwa. Aligned reads were parsed and UMIs were counted for each gene in each sample to create an expression matrix containing the absolute abundance of mRNAs in all samples. Reads aligned on multiple genes or containing more than 3 mismatches with the reference were discarded. The expression matrix was normalized and differentially expressed genes (DEG) were searched using the R package deseq2 (doi: 10.1186/s13059-014-0550-8). If DEG were found, functional annotation was performed using the R package ClusterProfiler (doi: 10.1016/j.xinn.2021.100141 / doi: 10.1089/omi.2011.0118).

Generation of Lentiviral vectors:

For RNA interference, the sequence for non-target shRNA was previously described (KY Lee et al 2016) (Table 1). For Arhgef18, specific sense and anti-sense DNA sequences were identified using free online services (http://sidirect2.rnai.jp/; http://web.stanford.edu/group/markkaylab/cgi-bin/)[1] (Gu et al. 2014). The sequences that met the optimal criteria were selected and synthesized as oligos in the form of miR-E backbone. The oligos were then amplified using the primers miRE-fw (5'-TGAACTCGAGAAGGTATATTGCTGTTGACAGTGAGCG-3'), miRE-Rv (5'-TCTCGAATTCTAGCCCCTTGAAGTCCGAGGCAGTAGGC-3') and Q5 Hot Start High-Fidelity DNA polymerase (NEB M049S). The final amplicon was then digested and cloned into LT3GEPIR in-between XhoI and EcoRI restriction sites as previously described[2]. The cloned shRNAs were sequence confirmed using the primer miRseq5 (5'-TGTTTGAATGAGGCTTCAGTAC-3'). The resultant lentiviral vector drives the expression of shRNA along with EGFP under TRE3G promoter, a doxycycline inducible promoter.

For Arhgef18 overexpression constructs, Arhgef18 was amplified from HUVEC cDNA by overlap-extension PCR using the following oligos and primers (Table 2). The resultant amplicon was digested and clone into LT3(AsiSI)N1-GPIR (modified LT3GEPIR) vector in between AsiSI and EcoRI restriction sites. The resultant vector LT3N1-GPIR-Arhgef18 encodes Arhgef18-EGFP fusion protein under TRE3G promoter. GEF mutant version of Arhgef18 was generated by site directed mutagenesis of tyrosine to alanine at amino acid position 260 using primers A18-Y260A-SDM-Fr (5'-CATAACCAAAGCCCCAGTGCTGGTG-3'), A18-Y260A-SDM-Rev (5'-CGTTGTGTAACCAGGAGAATG-3') and Q5 site directed mutagenesis kit (NEB E0554). This LT3N1-GPIR-Arhgef18 vectors were further modified to substitute EGFP with 3XHA-FLAG tag, shArhgef18.6 to target endogenous Arhgef18 and P2A sequence to replace IRES using standard molecular cloning techniques. The resultant vector is designated as Arhgef18-HA/FLAG_shArhgef18.6.

Lentivirus production, transduction and induction of gene of interest vectors

Lentivirus vector carrying either the shRNA or Arhgef18 ORF was transfected into HEK293T cells along with packaging vectors psPAX2 and pVSVG2 (provided by Prof. Dr.Utz Fischer's lab) using polyethylenimine (764965; Sigma-Aldrich) transfection agent. After overnight incubation, the medium was replaced with fresh medium (DMEM+10%serum+PenStrep). Forty-eight hours and 72 h after transfection, viral supernatant was collected, filtered through 0.22 µm filter and used to infect HUVECs (passage 2) in the presence of polybrene (8 µg/ml, H9268; Sigma-Aldrich). The transduced HUVECs were selected with puromycin (8ug/ml, P8833; Sigma-Aldrich) for 48 h and maintained in the presence of puromycin (1µg/ml). The induction of either shRNA or full length Arhgef18 was performed at least 2days before the experiment by supplementing the medium with doxycycline (1µg/ml, D9891; Sigma-Aldrich) and maintained throughout the experimental procedure.

Pulldown Assay

Pulldown of active small GTPases (RhoA/Rac) or active Arhgef18 was done as previously described[3]. Briefly, HUVECs (WT, shRNA or A18-Y260A) subjected to various shear stress conditions for indicated time, were lysed in either RBD lysis buffer (50 mM Tris-HCl (pH 7.6), 500 mM NaCl, 1% (vol/vol) Triton X-100, 0.1% (wt/vol) SDS, 0.5% (wt/vol) deoxycholate and 10 mM MgCl2) or GEF lysis buffer (20 mM HEPES pH 7.5, 150 mM NaCl, 5 mM $MgCl_2$, 1% (vol/vol) Triton X-100, 1 mM DTT) supplemented with protease and phosphatase inhibitor cocktail. Cell debris was removed by centrifugation and equal volumes of cell lysate was incubated with 25-50 ug of either GST-RBD/PBD for active small-GTPases; or GST tagged RhoAG17A/Rac1G15A for active GEF pulldown for 45min. After incubation, beads were washed twice in respective wash buffers. Captured proteins were detected using Western Blot.

Co-immunoprecipitation assay

HUVECs (WT) subjected to various shear stress conditions for indicated time, were lysed in RBD lysis buffer (50 mM Tris-HCl (pH 7.6), 500 mM NaCl, 1% (vol/vol) Triton X-100, 0.1% (wt/vol) SDS, 0.5% (wt/vol) deoxycholate and 10 mM MgCl2) supplemented with protease and phosphatase inhibitor cocktail. Lysis buffer was homogenized passing through a 32-gauge syringe needle and cellular debris were removed by centrifugation (5 min, 10000 rpm). A small amount of the lysate was collected in order to assess the presence of the protein in the total cell lysate. Beads were first equilibrated in RBD buffer and then coated with 0.5 µg of the following antibodies: Claudin5 (genentex), ZO-1 (Thermofisher), VE-cadherin (R&D systems), Paxillin (Abcam). Cell lysats were then incubated with the coated beads, supernatants and immunoprecipitats (washed 3 times) were stored to proceed for Western blot.

Micropatterning assay

Pattern shape was design with FIJI software to have a L shaped pattern 50x50µm long and 6µm large. PDMS stencils were placed in IBIDI wells and cleaned in a Plasma cleaner for 5 min. A hydrophobic treatment was done using PLL PEG (Poly-lysine Polyethylene glycol 100µg/ml) for 30min. Wells were washed 3 times with PBS. Patterns were then prepared using the Primo device (Alveole). Briefly, the wells with PLPP (photoinitiator, Alveole) were placed under a microscope with the PRIMO device. focus was adjusted to UV reflection and the patterning sequence was launched with 1200mJ/mm2 UV exposure. Once patterned, wells were profusely washed with PBS and then coated with fibronectin (10µg/ml). Six hundred cells were seeded per well for 1h, then washed and the remaining cells were left to adhere for 12 h.

Western blotting

HUVECs were washed with cold PBS and scraped off in NETF buffer supplemented with protease and phosphatase inhibitors. Lysates were centrifuged and protein supernatant was quantified using the

Lowry protein assay (Bio-Rad). Lysates were reduced in lamelli buffer and electrophoresis was performed using precast SDS-PAGE gels (Biorad) and transferred on to PVDF membranes (Biorad). Equal loading was checked using Ponceau red solution. Membranes were then blocked in 5% milk and probed with primary antibodies over-night (see below) and respective secondary antibodies (1:3000). The membranes were developed using ECL (Biorad) using the Chemidoc imaging system (Biorad). After initial immunodetection, membranes were re-probed with anti–GAPDH antibody. The protein bands were quantified using fiji and expressed as a relative value to either GAPDH or as the ratio of phosphorylated to total protein. The following antibodies were used: ARHGEF18 (1/500; GTX102223; Genetex), p38 (1:500; 9212, CST), Phospho-p38 (1:500; 9211, CST) ERK1/2 (1:500; 4695, CST), phospho-ERK1/2 (1:500; 9101, CST), Akt (1:500; 9272, CST), phospho-Akt (1:500; 9271, CST), Claudin5 (1:500; 34-1600, Invitrogen), RhoA (1:500; 2117, CST), Rac1 (1:500; 2465, CST), Vav (1:250; ab92890; abcam), GST (1:2000; PC53-100UG; Oncogene), paxillin (1:500; ab32084; abcam), phospho-paxillin (1:500; ab194738; abcam), GAPDH (1:1000; MAB374, MerckMillipore).

In vitro Immunofluorescence staining

HUVECs were fixed with 4% PFA in PBS for 10 min at room temperature (RT). Blocking/ permeabilization was performed using blocking buffer consisting of 5% BSA (Sigma-Aldrich), 0.5% Triton X-100 (Sigma-Aldrich), 0.01% sodium deoxycholate (Sigma-Aldrich), and 0.02% sodium azide (Sigma-Aldrich) in PBS at pH 7.4 for 45 min at RT. Primary antibodies were incubated at the desired concentration in 1:1 Blocking buffer/PBS at RT for 2 hours and secondary antibodies (Life Technologie, Alexa, 1/500) were incubated at the desired concentration in 1:1 blocking buffer/PBS for 1 hour at RT. DAPI (Sigma-Aldrich, 1/10000, 5 min) was used for nuclear labeling and phaloidin488 (life technologies, 1/500, 45min) was used to labelled polymerized actin. The following antibodies were used in vitro: VE-Cadherin (1/1000, RandD), ZO-1 (1/500, 61-7300, life technologies), claudin5 (MAB19903, Abnova, 1/500), paxillin (Abcam, 1/1000),

In vivo Immunofluorescence staining

Retinas were fixed with 4% PFA in PBS overnight at 4°C. Blocking/ permeabilization was performed using blocking buffer consisting of 1% FBS, 3% BSA (Sigma-Aldrich), 0.5% Triton X-100 (Sigma-Aldrich), 0.01% sodium deoxycholate (Sigma-Aldrich), and 0.02% sodium azide (Sigma-Aldrich) in PBS at pH 7.4 for 1 hour at RT. Anti-ARHGEF18 antibody was incubated at 1/400 in 1:1 Blocking buffer/PBS overnight at 4°C and secondary antibody (anti-rabbit 568, life technologies, 1/400) was incubated in 1:1 blocking buffer/PBS for 2 hours at RT. DAPI (Sigma-Aldrich, 1/10000, 5 min) was used for nuclear labeling and Isolectin B4 488 (life technologies, 1/400, 1h) was used to labelled endothelial cells. Retinas were mounted in Mowiol.

Impedance-based assay

Cell adhesion assay was performed using xCELLigence RTCA instrument (Roche). Briefly, HUVECs (P4-P6) expressing either shNT (non-target), sh18.1 or sh18.4 were plated in E-plate 96 well (5232368001; Agilent) at a density of 20,000cells/well. Cell adhesion was measured as electrical impedance between electrodes and represented as cell index value over a period of time.

Permeability assay

HUVECs expressing shRNAs were plated onto 0.4 μm trans-well inserts (353095; Corning) coated with 0.2% gelatin (G1393; Sigma-Aldrich). Once the cells form a confluent monolayer, fluorescent dextran dyes 3 kDa and 70 kDa (D3329, D1540 respectively; Thermofisher) were added to the top chamber at a concentration of 1 mg/ml. Medium from lower chamber was collected at different time points. Fluorescence (Ex 595nm, Em 615nm for D3329; Ex 570nm, Em 590nm for D1540) was measured using Varioskan LUX (Thermofisher).

Wound healing assay

Confluent monolayer of HUVECs were scratched using a pipette tip. Cell debris were washed and the medium was replaced with fresh complete medium. Cell migration was videorecorded under optimal conditions (37ºC and 5%CO2) using an inverted Ti Eclipse microscope equipped with a 10x/0.25 phase contrast objective and a DS-Qi2 CMOS camera (Nikon France, Champigny Sur Marne). Images were recorded every 5 minutes during 24h. Wound area was manually measured at different time points using Fiji and rate of wound closure was calculated by area relative to time.

Matrigel assay

Network formation assay was performed on Matrigel (354230; Corning) in 96 well plate. HUVECs were

plated on Matrigel at a density of 15000 cells per well in complete medium. The network formation was photographed at 20 min interval for 24 h using JuLi Stage microscope and analyzed using Fiji macro (Angiogenesis analyzer).

Proliferation assay
Proliferation assay was performed using the Edu-click647 kit (BCK-EdU647; Base Click). HUVECs expressing the shRNAs were plated in µ-Slide VI 0.4 (80606; IBIDI) at a density of 30,000cells per channel in starving medium (EBM+0.5%serum+doxy+puro). After 16 h, cells were stimulated with complete medium (EBM+2%serum+doxy+puro) in the presence of EdU (5uM) under static or flow for 8 h. Cells were fixed in 4%formaldehyde for 10 min, stained for EdU and nuclei were labeled with DAPI (62248; Thermofisher) according to the kit manual. DAPI+ and EdU+ cells were counted using Fiji.

Microscope image acquisition
Images from fluorescently labeled HUVECs were acquired using a confocal A1 SIM microscope (Nikon) equipped with a Plan-Apochromat 20×/0.8 NA Ph2 objective or with a 60x/1.4 plan apochromat objective ; or using an Eclipse Ti2 inverted microscope (Nikon). Images were taken at room temperature using NIS Element software. Images of Retinas and Aortas were taken using a LFOV FLIM inverted confocal microscope (Nikon) equipped with a Plan-Apochromat 20×/0.8 NA Ph2 objective or with a Plan-Apochromat 60×/1.4 NA DIC objective. The microscope was equipped with a photon multiplier tube detector. Images were taken at room temperature using NIS element software (Nikon).

Flow-induced orientation analysis
Cell shape was quantified using a dedicated FIJI macro. Basically, VE-Cadherin staining was detected in order to segment the border of each endothelial cell. Based on this segmentation a skeleton was built and aspect ratio (major axis lenght by minor axis lenght, AR) as well as the angle between the flow direction and the main axis was determined for all entire ECs visible on the image. Flow index corresponding to the ratio of AR and the angle was calculated for each EC. Flow index thus integrates both the elongation and the alignment of endothelia cells: The higher the flow index is, the better the cell response to the flow. Based on the VE-cadherin staining, gaps in the endothelial monolayer were quantified manually, only gaps with an area above 100um were taken in account.

Cell junction activity analysis
ZO-1 intensity at the junctions was quantified using FIJI. Briefly, an enlarged mask from the VE-Cadherin segmentation previously described was generated and applied on the ZO-1 staining image, percentage of the ZO-1 staining in this area was extracted for each image. Actin cable formation was measured by the intensity of the phalloidin staining at the junctions using the same enlarged mask applied on the Actin staining image (FIJI). Both analyses were made automatically by FIJI with identical parameter for mask enlargement and threshold values. Claudin5 localization at junction was quantified using a mix of ECs expressing or not the shRNA targeting ARHGEF18. Using FIJI, Intensity plots for both Claudin5 and VE-cadherin staining were obtained by drawing a line of approximately 15um in between two cells.

Basal adhesion analysis
For micropatterning images, paxillin channel was thresholded and the focal adhesion length was quantified for each focal adhesion detected. The focal adhesions were then classified by size within each cell. Quantification was done blindly.
For shear stress exposed ECs, focal adhesion type was assessed qualitatively by classifying blindly (by 2 operators) the overall aspect of Paxillin staining in the cell. Cells with long, numerous and parallel focal adhesions were classified 1 and cells with short, few and disorganized focal adhesions were classified 0.

Statistical analysis
Statistical analysis was performed using GraphPad Prism software. For in vitro and in vivo experiments, when only 2 conditions were compared, a paired T-test or a Wilcoxon T-test were used depending on the distribution of the data. For multiple comparison an ordinary one-way ANOVA (data distribution was assumed to be normal) was used, followed by a Tukey test. Details of the statistical test used for each experiment can be found in the figure legends.

Bibliography

1. Ui-Tei, K. *et al.* Guidelines for the selection of highly effective siRNA sequences for mammalian and chick RNA interference. *Nucleic Acids Res.* **32**, 936–948 (2004).
2. Fellmann, C. *et al.* An optimized microRNA backbone for effective single-copy RNAi. *Cell Rep.* **5**, 1704–1713 (2013).
3. Guilluy, C., Dubash, A. D. & García-Mata, R. Analysis of RhoA and Rho GEF activity in whole cells and the cell nucleus. *Nat. Protoc.* **6**, 2050–2060 (2011).
4. Ingber, D. E. Cellular mechanotransduction: putting all the pieces together again. *FASEB J. Off. Publ. Fed. Am. Soc. Exp. Biol.* **20**, 811–827 (2006).
5. Ballermann, B. J., Dardik, A., Eng, E. & Liu, A. Shear stress and the endothelium. *Kidney Int. Suppl.* **67**, S100-108 (1998).
6. Hahn, C. & Schwartz, M. A. Mechanotransduction in vascular physiology and atherogenesis. *Nat. Rev. Mol. Cell Biol.* **10**, 53–62 (2009).
7. Wang, C., Baker, B. M., Chen, C. S. & Schwartz, M. A. Endothelial cell sensing of flow direction. *Arterioscler. Thromb. Vasc. Biol.* **33**, 2130–2136 (2013).
8. Givens, C. & Tzima, E. Endothelial Mechanosignaling: Does One Sensor Fit All? *Antioxid. Redox Signal.* **25**, 373–388 (2016).
9. Galie, P. A. *et al.* Fluid shear stress threshold regulates angiogenic sprouting. *Proc. Natl. Acad. Sci. U. S. A.* **111**, 7968–7973 (2014).
10. Franco, C. A. *et al.* Non-canonical Wnt signalling modulates the endothelial shear stress flow sensor in vascular remodelling. *eLife* **5**, e07727 (2016).
11. Daems, M., Peacock, H. M. & Jones, E. A. V. Fluid flow as a driver of embryonic morphogenesis. *Dev. Camb. Engl.* **147**, dev185579 (2020).
12. Lu, D. & Kassab, G. S. Role of shear stress and stretch in vascular mechanobiology. *J. R. Soc. Interface* **8**, 1379–1385 (2011).
13. Tzima, E. *et al.* A mechanosensory complex that mediates the endothelial cell response to fluid shear stress. *Nature* **437**, 426–431 (2005).
14. Chiu, J.-J. & Chien, S. Effects of disturbed flow on vascular endothelium: pathophysiological basis and clinical perspectives. *Physiol. Rev.* **91**, 327–387 (2011).
15. Chalouhi, N., Hoh, B. L. & Hasan, D. Review of cerebral aneurysm formation, growth, and rupture. *Stroke* **44**, 3613–3622 (2013).
16. Tzima, E. *et al.* Activation of Rac1 by shear stress in endothelial cells mediates both cytoskeletal reorganization and effects on gene expression. *EMBO J.* **21**, 6791–6800 (2002).
17. Pan, S. Molecular mechanisms responsible for the atheroprotective effects of laminar shear stress. *Antioxid. Redox Signal.* **11**, 1669–1682 (2009).
18. Hoger, J. H., Ilyin, V. I., Forsyth, S. & Hoger, A. Shear stress regulates the endothelial Kir2.1 ion channel. *Proc. Natl. Acad. Sci. U. S. A.* **99**, 7780–7785 (2002).
19. Vion, A.-C. *et al.* Primary cilia sensitize endothelial cells to BMP and prevent excessive vascular regression. *J. Cell Biol.* **217**, 1651–1665 (2018).
20. Van der Heiden, K. *et al.* Endothelial primary cilia in areas of disturbed flow are at the base of atherosclerosis. *Atherosclerosis* **196**, 542–550 (2008).
21. Goldfinger, L. E. *et al.* Localized alpha4 integrin phosphorylation directs shear stress-induced endothelial cell alignment. *Circ. Res.* **103**, 177–185 (2008).
22. Tzima, E. Role of small GTPases in endothelial cytoskeletal dynamics and the shear stress response. *Circ. Res.* **98**, 176–185 (2006).
23. Boon, R. A. *et al.* KLF2-induced actin shear fibers control both alignment to flow and JNK signaling in vascular endothelium. *Blood* **115**, 2533–2542 (2010).
24. Girard, P. R. & Nerem, R. M. Shear stress modulates endothelial cell morphology and F-actin organization through the regulation of focal adhesion-associated proteins. *J. Cell. Physiol.* **163**, 179–193 (1995).

25. Levesque, M. J. & Nerem, R. M. The elongation and orientation of cultured endothelial cells in response to shear stress. *J. Biomech. Eng.* **107**, 341–347 (1985).
26. Malek, A. M. & Izumo, S. Mechanism of endothelial cell shape change and cytoskeletal remodeling in response to fluid shear stress. *J. Cell Sci.* **109 (Pt 4)**, 713–726 (1996).
27. Wojciak-Stothard, B. & Ridley, A. J. Shear stress-induced endothelial cell polarization is mediated by Rho and Rac but not Cdc42 or PI 3-kinases. *J. Cell Biol.* **161**, 429–439 (2003).
28. Tzima, E., del Pozo, M. A., Shattil, S. J., Chien, S. & Schwartz, M. A. Activation of integrins in endothelial cells by fluid shear stress mediates Rho-dependent cytoskeletal alignment. *EMBO J.* **20**, 4639–4647 (2001).
29. Li, S. *et al.* Distinct roles for the small GTPases Cdc42 and Rho in endothelial responses to shear stress. *J. Clin. Invest.* **103**, 1141–1150 (1999).
30. Etienne-Manneville, S. & Hall, A. Rho GTPases in cell biology. *Nature* **420**, 629–635 (2002).
31. Rossman, K. L., Der, C. J. & Sondek, J. GEF means go: turning on RHO GTPases with guanine nucleotide-exchange factors. *Nat. Rev. Mol. Cell Biol.* **6**, 167–180 (2005).
32. Cook, D. R., Rossman, K. L. & Der, C. J. Rho guanine nucleotide exchange factors: regulators of Rho GTPase activity in development and disease. *Oncogene* **33**, 4021–4035 (2014).
33. Cheng, C. *et al.* Endothelial cell-specific FGD5 involvement in vascular pruning defines neovessel fate in mice. *Circulation* **125**, 3142–3158 (2012).
34. Liu, Y. *et al.* A novel pathway spatiotemporally activates Rac1 and redox signaling in response to fluid shear stress. *J. Cell Biol.* **201**, 863–873 (2013).
35. Kroon, J. *et al.* Flow-induced endothelial cell alignment requires the RhoGEF Trio as a scaffold protein to polarize active Rac1 distribution. *Mol. Biol. Cell* **28**, 1745–1753 (2017).
36. Polacheck, W. J. *et al.* A non-canonical Notch complex regulates adherens junctions and vascular barrier function. *Nature* **552**, 258–262 (2017).
37. Lessey-Morillon, E. C. *et al.* The RhoA guanine nucleotide exchange factor, LARG, mediates ICAM-1-dependent mechanotransduction in endothelial cells to stimulate transendothelial migration. *J. Immunol. Baltim. Md 1950* **192**, 3390–3398 (2014).
38. García-Mata, R. *et al.* Analysis of activated GAPs and GEFs in cell lysates. *Methods Enzymol.* **406**, 425–437 (2006).
39. Terry, S. J. *et al.* Spatially restricted activation of RhoA signalling at epithelial junctions by p114RhoGEF drives junction formation and morphogenesis. *Nat. Cell Biol.* **13**, 159–166 (2011).
40. Garrett, T. A., Van Buul, J. D. & Burridge, K. VEGF-induced Rac1 activation in endothelial cells is regulated by the guanine nucleotide exchange factor Vav2. *Exp. Cell Res.* **313**, 3285–3297 (2007).
41. Zaritsky, A. *et al.* Diverse roles of guanine nucleotide exchange factors in regulating collective cell migration. *J. Cell Biol.* **216**, 1543–1556 (2017).
42. Loie, E., Charrier, L. E., Sollier, K., Masson, J.-Y. & Laprise, P. CRB3A Controls the Morphology and Cohesion of Cancer Cells through Ehm2/p114RhoGEF-Dependent Signaling. *Mol. Cell. Biol.* **35**, 3423–3435 (2015).
43. Kim, M., M Shewan, A., Ewald, A. J., Werb, Z. & Mostov, K. E. p114RhoGEF governs cell motility and lumen formation during tubulogenesis through a ROCK-myosin-II pathway. *J. Cell Sci.* **128**, 4317–4327 (2015).
44. Rousseau, S. *et al.* Vascular endothelial growth factor (VEGF)-driven actin-based motility is mediated by VEGFR2 and requires concerted activation of stress-activated protein kinase 2 (SAPK2/p38) and geldanamycin-sensitive phosphorylation of focal adhesion kinase. *J. Biol. Chem.* **275**, 10661–10672 (2000).

45. Kanaji, N. *et al.* The p38 mitogen-activated protein kinases modulate endothelial cell survival and tissue repair. *Inflamm. Res. Off. J. Eur. Histamine Res. Soc. Al* **61**, 233–244 (2012).
46. Lee, J. *et al.* p85 beta-PIX is required for cell motility through phosphorylations of focal adhesion kinase and p38 MAP kinase. *Exp. Cell Res.* **307**, 315–328 (2005).
47. Ni, Y. *et al.* TNFα alters occludin and cerebral endothelial permeability: Role of p38MAPK. *PloS One* **12**, e0170346 (2017).
48. Langille, B. L. Morphologic responses of endothelium to shear stress: reorganization of the adherens junction. *Microcirc. N. Y. N 1994* **8**, 195–206 (2001).
49. Bahrami, S. & Drabløs, F. Gene regulation in the immediate-early response process. *Adv. Biol. Regul.* **62**, 37–49 (2016).
50. Kilian, L. S., Voran, J., Frank, D. & Rangrez, A. Y. RhoA: a dubious molecule in cardiac pathophysiology. *J. Biomed. Sci.* **28**, 33 (2021).
51. Sumpio, B. E. *et al.* MAPKs (ERK1/2, p38) and AKT can be phosphorylated by shear stress independently of platelet endothelial cell adhesion molecule-1 (CD31) in vascular endothelial cells. *J. Biol. Chem.* **280**, 11185–11191 (2005).
52. Azuma, N. *et al.* Role of p38 MAP kinase in endothelial cell alignment induced by fluid shear stress. *Am. J. Physiol. Heart Circ. Physiol.* **280**, H189-197 (2001).
53. Nakajima, H. & Tanoue, T. Lulu2 regulates the circumferential actomyosin tensile system in epithelial cells through p114RhoGEF. *J. Cell Biol.* **195**, 245–261 (2011).
54. Blomquist, A. *et al.* Identification and characterization of a novel Rho-specific guanine nucleotide exchange factor. *Biochem. J.* **352 Pt 2**, 319–325 (2000).
55. Herder, C. *et al.* ArhGEF18 regulates RhoA-Rock2 signaling to maintain neuro-epithelial apico-basal polarity and proliferation. *Dev. Camb. Engl.* **140**, 2787–2797 (2013).
56. Niu, J., Profirovic, J., Pan, H., Vaiskunaite, R. & Voyno-Yasenetskaya, T. G Protein betagamma subunits stimulate p114RhoGEF, a guanine nucleotide exchange factor for RhoA and Rac1: regulation of cell shape and reactive oxygen species production. *Circ. Res.* **93**, 848–856 (2003).
57. Lawson, C. D. & Burridge, K. The on-off relationship of Rho and Rac during integrin-mediated adhesion and cell migration. *Small GTPases* **5**, e27958 (2014).
58. Acharya, B. R. *et al.* A Mechanosensitive RhoA Pathway that Protects Epithelia against Acute Tensile Stress. *Dev. Cell* **47**, 439-452.e6 (2018).
59. Haas, A. J. *et al.* Interplay between Extracellular Matrix Stiffness and JAM-A Regulates Mechanical Load on ZO-1 and Tight Junction Assembly. *Cell Rep.* **32**, 107924 (2020).
60. Tornavaca, O. *et al.* ZO-1 controls endothelial adherens junctions, cell-cell tension, angiogenesis, and barrier formation. *J. Cell Biol.* **208**, 821–838 (2015).
61. Carvalho, J. R. *et al.* Non-canonical Wnt signaling regulates junctional mechanocoupling during angiogenic collective cell migration. *eLife* **8**, (2019).
62. Birukova, A. A., Shah, A. S., Tian, Y., Moldobaeva, N. & Birukov, K. G. Dual role of vinculin in barrier-disruptive and barrier-enhancing endothelial cell responses. *Cell. Signal.* **28**, 541–551 (2016).
63. Beal, R., Alonso-Carriazo Fernandez, A., Grammatopoulos, D. K., Matter, K. & Balda, M. S. ARHGEF18/p114RhoGEF Coordinates PKA/CREB Signaling and Actomyosin Remodeling to Promote Trophoblast Cell-Cell Fusion During Placenta Morphogenesis. *Front. Cell Dev. Biol.* **9**, 658006 (2021).